Velocity correction for the Actuator Line Method

Davide Selvatici[1] and Richard J.A.M. Stevens[1]

[1]Physics of Fluids Group, Max Planck Center Twente for Complex Fluid Dynamics, J. M. Burgers Center for Fluid Dynamics, University of Twente, P. O. Box 217, Enschede 7500 AE, Netherlands

Correspondence: Davide Selvatici (d.selvatici@utwente.nl) and Richard J.A.M. Stevens (r.j.a.m.stevens@utwente.nl)

Abstract. We introduce a velocity correction designed to mitigate the overestimation of aerodynamic loads observed with the traditional Actuator Line Method (ALM) at the blades tip. The correction is based on Blade Element Momentum (BEM) theory to determine the ratio of tip-corrected to non-tip-corrected axial and tangential velocity components. These velocity ratios are used to correct the velocities at the blade locations, ensuring an accurate representation of aerodynamic effects near the blade

5   tips. The correction only requires the Tip Speed Ratio (TSR), which can be estimated from local flow conditions and turbine specifications. This makes the method highly adaptable to various flow scenarios. The effectiveness of the proposed correction has been validated through Large Eddy Simulations (LES) at multiple inflow velocities through comparison against both BEM with tip correction and a vortex-based smearing correction for ALM.

1   Introduction

10   Numerical simulations of wind turbines frequently employ the Actuator Line Method (ALM) as introduced by Sørensen and Shen (2002). ALM computes instantaneous turbine blade loading by leveraging tabulated lift and drag characteristics of the blades. The forces on the wind turbine blades are integrated into a Navier-Stokes solver, which enables accurate representation of wake dynamics. Liu et al. (2022) demonstrated that with sufficient grid refinement, ALM can approximate the loading distributions predicted by the Blade Element Momentum (BEM) theory without tip correction. However, the absence of tip

15   correction in BEM leads to inaccuracies in simulating the pressure equalization observed at the blade tip in blade-resolved simulations and experimental investigations (Glauert, 1935; Branlard, 2017; Bangga and Lutz, 2021; Madsen et al., 2010; Bangga, 2018). Consequently, including tip corrections has become a standard practice in BEM to address these discrepancies (Branlard, 2017; Sørensen, 2016).

Several strategies have been explored to reduce the overestimation of tip loads in ALM. Shen et al. (2005) suggested applying

20   the tip correction directly to the force distribution on the blades. However, it has been noted that this method results in the underestimation of blade loading when applied to coarse mesh simulations (Dağ and Sørensen, 2019). Moreover, this approach does not account for the influence of tip corrections on the angle of attack and induction factors, both of which are essential for achieving results that are consistent with BEM theory.

In the classical ALM framework, forces on the blades are distributed by employing a Gaussian projection function, wherein

25   the projection radius ε is set to twice the grid spacing to ensure numerical stability. Using potential flow theory in two-dimensional flows, it has been shown that the physically optimal value ε depends on the chord length of the blade (Martínez-

Tossas et al., 2017). Simulations using a radius-dependent ε, particularly decreasing ε towards the blade tip, have yielded improvements in blade loading (Jha et al., 2014; Jha and Schmitz, 2017; Churchfield et al., 2017). However, this technique necessitates a very fine grid resolution, as small as 15 cm at the blade tip, to effectively become an accurate tip correction.

30   Dağ and Sørensen (2019) identified that the overestimation of tip loading in ALM originates from an overestimation of the angle of attack or, equivalently, of the sampled velocity at the blades from which the angle of attack is computed. This recognition led to the development of a vortex-based smearing correction method. The technique was further advanced by Meyer Forsting et al. (2019, 2020), who propose a smearing correction based on empirical coefficients (Pirrung et al., 2017) to reduce the computational overhead of the method. They conclude that this method accurately reflects blade loading obtained

35   from the Lifting Line theory, even on coarser meshes.

Given the success of the vortex-based smearing correction method, we conclude that correcting the sampled velocity at the blade location is crucial. Using this insight, we propose a novel adjustment to the classical ALM by using BEM to perform the tip corrections. The proposed algorithm benefits from its straightforward implementation, minimal computational overhead, and consistency with the widely used BEM framework, which ensures broad applicability.

40   The remainder of this manuscript is structured as follows: Section 2 discusses tip corrections within BEM theory, and Section 3 reviews the classical ALM implementation. Section 4 introduces the proposed ALM correction method, and Section 5 describes the numerical details of the Large Eddy Simulations (LES) that are used to evaluate the proposed method. Section 6 validates the proposed method against the BEM with tip correction and the vortex-based smearing correction (Meyer Forsting et al., 2019, 2020). In section 6.4 we study the effect of different inflow velocity conditions. Lastly, Section 7 summarizes the

45   work.

2   Tip-corrections in blade element momentum theory

BEM theory is an analytic approach that has been developed to evaluate the loading on wind turbine blades. It is based on the equivalence between the blade element and axial momentum theory, making it possible to compute the induction velocity and loads at the rotor; see Branlard (2017); Sørensen (2016) for detailed discussions on BEM. Here, we focus on the tip correction

50   function typically adopted to consider three-dimensional effects at the blade tips. The tip correction function was derived by Prandtl and Glauert using potential flow theory to account for the deflection of the flow streamlines when a finite number of blades is considered (Branlard, 2017). The most common tip correction formulation is

$$F(r) = \frac{2}{\pi} \cos^{-1} \left(\exp \left(-\frac{B(R-r)}{2r \sin \phi} \right) \right), \tag{1}$$

where B is number of blades, R is the blades radius, r is the radial coordinate, and ϕ is the wind angle, defined as

55    $$\phi = \arctan \left(\frac{U}{V} \right), \tag{2}$$

with U and V the axial and tangential components of velocity at the blade (see figure 1):

$$U = U_\infty (1-a) \quad \text{and} \quad V = \Omega r (1+a'). \tag{3}$$
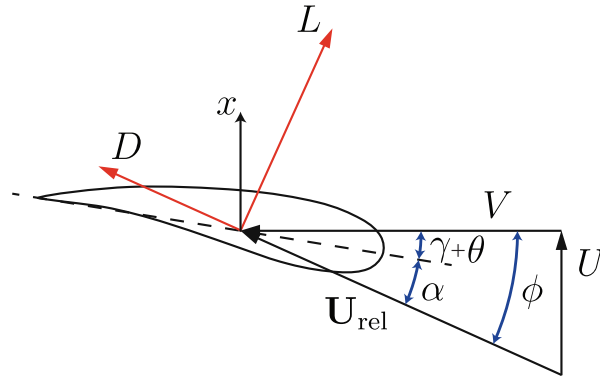
Figure 1. Sketch of the velocity components, angles, and forces as defined in BEM theory (Branlard, 2017). Flow direction is in positive x-direction.

where a and a' are the axial and tangential induction factors and Ω is the angular velocity of the rotor.

When the tip-loss function is adopted, the induction factors become dependent on the blade location (Branlard, 2017;
60 Sørensen, 2016):

$$a(r) = \frac{1}{\dfrac{4F(r)\sin^2\phi}{\sigma(r)C_n}+1} \quad \text{and} \quad a'(r) = \frac{1}{\dfrac{4F(r)\sin\phi\cos\phi}{\sigma(r)C_t}-1}, \tag{4}$$

in which $\sigma(r) = Bc(r)/(2\pi r)$ is the radially dependent solidity factor, $c(r)$ is the chord length, and $C_n(r)$ and $C_t(r)$ are the normal and tangential load coefficients, which are defined as

$$C_n(r) = C_L(r)\cos\phi + C_D(r)\sin\phi \quad \text{and} \quad C_t(r) = C_L(r)\sin\phi - C_D(r)\cos\phi \tag{5}$$

65 where $C_L(r)$ and $C_D(r)$ are the radially dependent lift and drag coefficients. Since $F(r)$ tends to 0 towards the tip, the induction factor increases. Therefore, the correction decreases the axial velocity and increases the tangential component. Given that the normal component of the velocity (C_n) at the blade tip significantly exceeds the tangential component (C_t), the relative increase in tangential velocity is smaller compared to the decrease in axial velocity. Consequently, this leads to a reduction in the load towards the blade tip.

70 The aerodynamic coefficients C_L and C_D are obtained from look-up tables that document the coefficients as a function of the angle of attack α, which is determined as (see figure 1)

$$\alpha(r) = \phi(r) - (\gamma(r) + \theta(r)), \tag{6}$$

where $\gamma(r)$ and $\theta(r)$ are the radially dependent twist and pitch angles of the blade.

The normal and tangential forces at the blade are obtained from the relative incoming velocity $U_\mathrm{rel} = \sqrt{U^2 + V^2}$ as:

75 $$F_n(r) = \frac{1}{2}\rho c U_\mathrm{rel}^2 C_n(r) \quad \text{and} \quad F_t(r) = \frac{1}{2}\rho c U_\mathrm{rel}^2 C_t(r). \tag{7}$$
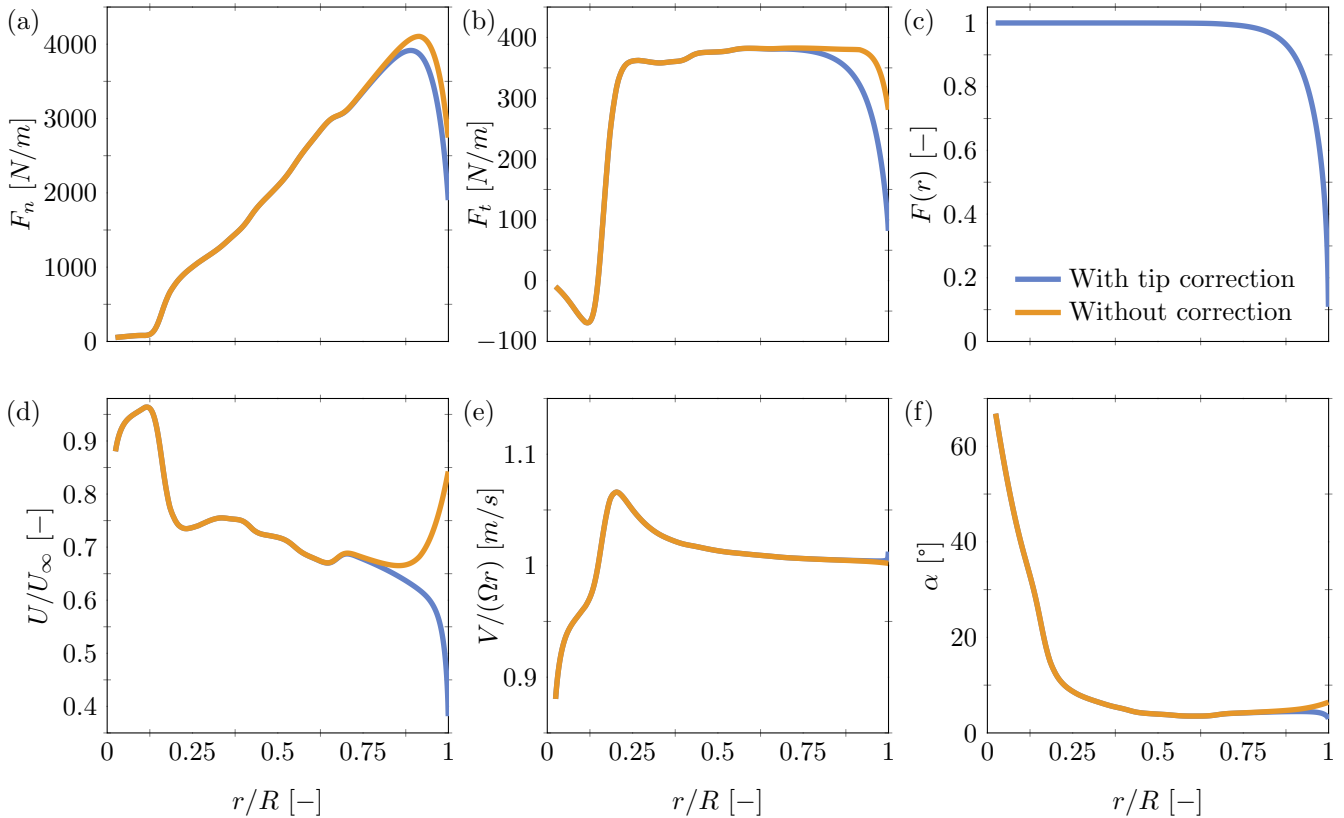
Figure 2. Comparison of (a,b) normal and tangential loads, (d,e) axial and tangential velocity component, and (f) angle of attack for BEM with and without tip correction. Panel c shows the tip correction function $F(r)$ (Eq. 1).

The rotor thrust and power coefficients follow from integration over the blades:

$$C_T = \frac{\int_{r_{\text{hub}}}^{R} F_n(r) \, B dr}{\frac{1}{2}\rho U_\infty^2 \pi R^2} \quad \text{and} \quad C_P = \frac{\int_{r_{\text{hub}}}^{R} F_t(r) \, rB\Omega dr}{\frac{1}{2}\rho U_\infty^3 \pi R^2}, \tag{8}$$

where r_{hub} is the hub radius.

We use the BEM implementation by Ning (2013), which guarantees convergence employing a one-dimensional residual function. Furthermore, for inductions greater than 0.4, we include the thrust-induction correction by Buhl (2005). To illustrate the effect of the tip correction, we consider the NREL-5MW rotor in a uniform inflow of 8 m/s and rotating at an angular velocity of 9.1552 rpm (Jonkman et al., 2009). Figure 2 reports the radial distribution of velocities and loadings along the blade, which confirms that tip correction effects are most evident in the axial velocity. Without tip correction, the normalized velocity increases towards the tip. With tip correction, the axial velocity decreases towards the tip due to the function F, which parametrizes the impact of three-dimensional effects such as tip vortices that deform and decelerate the flow behind the blade tips (Branlard, 2017; Glauert, 1935). Figure 2e illustrates that the tip correction has a limited impact on the tangential velocity
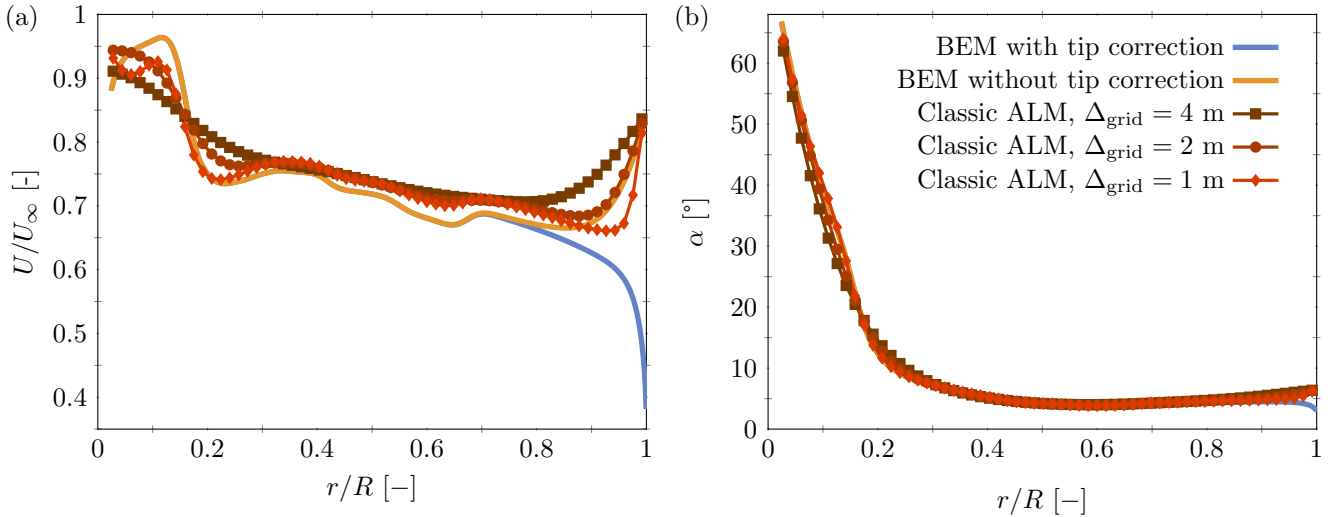
Figure 3. Comparison of the radial distributions of (a) axial velocity and (b) angle of attack between the classic ALM at grid spacings of $\Delta_{\mathrm{grid}} = 4, 2, 1$ m and BEM, both with and without tip correction.

V, which is primarily determined by the blade's rotational speed. The power and thrust coefficients with tip correction are $C_P = 0.4898$ and $C_T = 0.7892$. These values are 6.7% and 2.5% lower than those obtained without tip correction ($C_P = 0.5249$ and $C_T = 0.8096$).

3 Classic actuator line method

In ALM the blades are represented by lines discretized by points. A velocity vector is assigned to each blade point by interpolating the velocity field to the blade point and a smearing function distributes the computed forces to the grid points of the flow solver. Typically, a Gaussian projection

$$\eta(\boldsymbol{d}) = \frac{1}{\varepsilon^3 \pi^{3/2}} \exp\left(-\frac{|\boldsymbol{d}|^2}{\varepsilon^2}\right), \tag{9}$$

centered around the blade point, with $\boldsymbol{d}$ the distance from the blade point and $\varepsilon = 2\Delta_{\mathrm{grid}}$ the smearing radius, is employed (Sørensen and Shen, 2002; Troldborg, 2008; Martínez-Tossas et al., 2018). We sample the velocity at the blade location, which has the advantage of relating realistic flow features with the actuator points. Figure 3 presents a comparison of the axial velocity and angle of attack as obtained from ALM simulations with various grid resolutions with BEM theory. The figure illustrates that the ALM results converge towards BEM theory without tip correction. As shown by Melani et al. (2024), the sampling volume should decrease towards the tip to accurately capture the tip vortices and their effects on the loading. However, given that $\varepsilon = 2\Delta_{\mathrm{grid}}$, the mesh spacing required would still be beyond the lowest adopted here (i.e., 1 m) to appreciate improvements (Churchfield et al., 2017) and thus not feasible for large simulations. Therefore, the sampled velocity includes local fictitious

effects due to the load smearing that drive the axial velocity and the angle of attack to increase towards the tip, while they are expected to decrease (Melani et al., 2024; Churchfield et al., 2017; Meyer Forsting et al., 2019).

105 ## 4 ALM correction

We aim to ensure that the sampled velocity accurately reproduces the loads and the angle of attack distributions at the blade tip. Given the classic ALM convergence to BEM without tip correction, we employ BEM to calculate the ratio between the tip-corrected and sampled velocity. These ratios, $U_\text{tip}/U_\text{notip}$ for the axial component and $V_\text{tip}/V_\text{notip}$ for the tangential one, are used to determine the velocities at the blade tip. To achieve this, we express the wind angle ϕ as a function of the tip-speed
110 ratio (TSR). By incorporating the definition of the TSR

$$\text{TSR} = \frac{\Omega R}{U_\infty},\tag{10}$$

and equation 3 in the wind angle definition (equation 2), we obtain the following result

$$\phi = \arctan\left(\frac{U_\infty}{\Omega r}\frac{(1-a)}{(1+a')}\right) = \arctan\left(\frac{R/r}{\text{TSR}}\frac{(1-a)}{(1+a')}\right).\tag{11}$$

As shown by Diaz et al. (2023), the TSR can be estimated iteratively using the disk-averaged axial velocity U_d and C_T. In
115 particular, from the definition of C_T, a, and axial velocity (Eqs. 8, 4, and 3), one can derive that

$$U_\text{ref} = \frac{2\langle U_\text{d}\rangle}{1+\sqrt{1-C_T}}\tag{12}$$

$C_T = C_T(U_\text{ref})$ is the thrust coefficient as per turbine definition (see Jonkman et al. (2009) in the case of the NREL 5MW turbine), and the resulting tip-speed ratio is then $\text{TSR} = \Omega R/U_\text{ref}$, in which $\Omega = \Omega(U_\text{ref})$ is the angular velocity as per turbine definition. This enables the current method to be used even when the free-stream velocity is not directly accessible, for example,
120 within a wind farm.

Figure 4 shows how BEM can be used to compute the induction factors with and without tip correction with guaranteed convergence (Ning, 2013). Using the induction factors, the desired ratios $U_\text{tip}/U_\text{notip}$ and $V_\text{tip}/V_\text{notip}$ can be computed using:

$$\frac{U_\text{tip}}{U_\text{notip}} = \frac{1-a_\text{tip}}{1-a_\text{notip}} \quad \text{and} \quad \frac{V_\text{tip}}{V_\text{notip}} = \frac{1+a'_\text{tip}}{1+a'_\text{notip}}\tag{13}$$

The figure also shows how these corrected velocities are incorporated in classic ALM. The full algorithm consists of the
125 following points:

1. BEM is used to compute $U_\text{tip}/U_\text{notip}$ and $V_\text{tip}/V_\text{notip}$ using the TSR as the only input;

2. Compute the tip-corrected velocity components: $U_\text{c} = U \times U_\text{tip}/U_\text{notip}$ and $V_\text{c} = V \times V_\text{tip}/V_\text{notip}$;

3. Determine the relative velocity to the blade point: $U_\text{rel} = \sqrt{U_\text{c}^2 + V_\text{c}^2}$;

4. Determine the wind angle and angle of attack at the blade point using: $\phi = \arctan(U_\text{c}/V_\text{c})$, $\alpha = \phi - (\gamma + \theta)$;
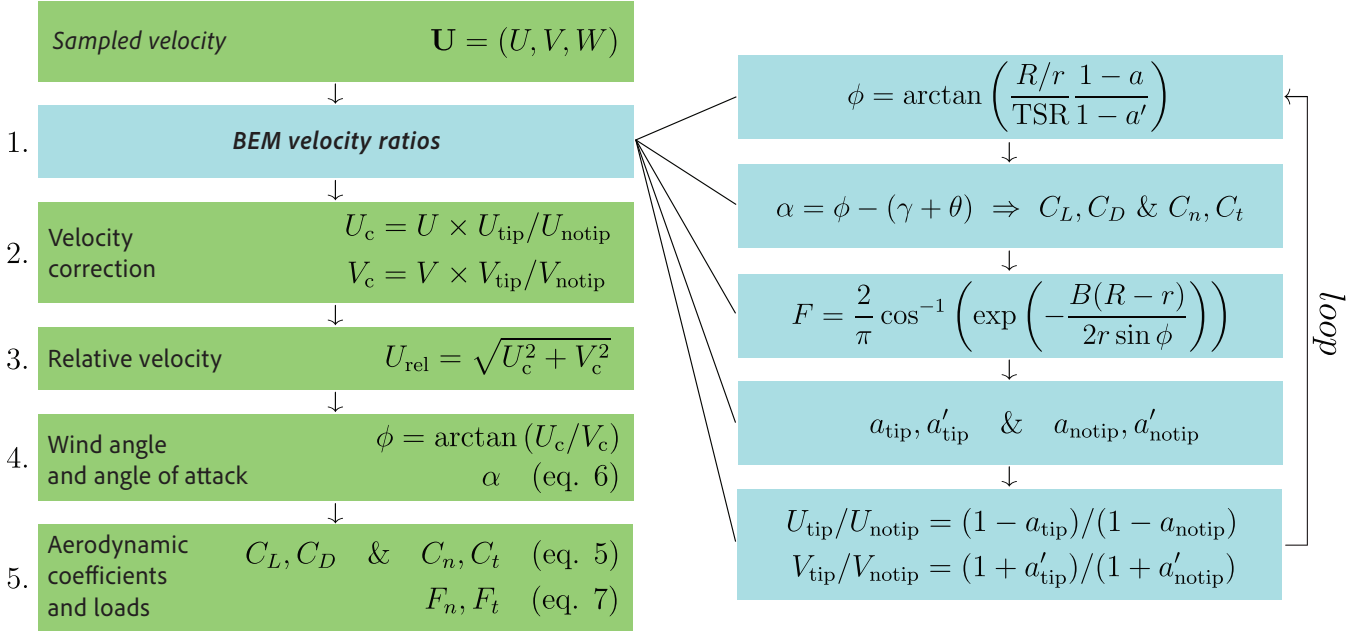
Figure 4. The diagram illustrates the proposed algorithm and its incorporation into the traditional ALM framework. Light-blue boxes illustrate the iterative loop to calculate the velocity ratios. Green boxes indicate the classic ALM steps. The velocity ratios that capture the tip corrections are incorporated in step 2.

5. By utilizing α and ϕ, the aerodynamic coefficients C_L, C_D, and C_n, C_t can be calculated (equation 5), which are used to calculate the loads (equation 7).

We note that the computational overhead compared to classic ALM is negligible when values from the previous timestep are used as initial guesses during the iteration procedure.

5 Large Eddy Simulation

We adopted an in-house pseudo-spectral LES based on Albertson (1996) and improved over the years (Stevens et al., 2014b, a; Gadde et al., 2021). The governing equations are the filtered continuity and momentum conservation equations:

$$\nabla \cdot \tilde{\boldsymbol{u}} = 0 \tag{14}$$

$$\frac{\partial \tilde{\boldsymbol{u}}}{\partial t} + \tilde{\boldsymbol{u}} \cdot \nabla \tilde{\boldsymbol{u}} = \boldsymbol{f}_{\mathrm{ALM}} - \nabla \tilde{p} - \nabla \cdot \boldsymbol{\tau}; \tag{15}$$

where $\boldsymbol{u}$ is the velocity vector, $\boldsymbol{f}_{\mathrm{ALM}}$ the forces on the blades calculated by the ALM, p is the kinematic pressure, and $\boldsymbol{\tau}$ is the sub-grid stresses (SGS) tensor. The tilde $\tilde{\cdot}$ indicates that a filtered velocity field is considered. The viscous stresses are neglected due to the large Reynolds number of atmospheric flows, and the SGS are modeled through $\tau_{ij} = \widetilde{u_i u_j} - \tilde{u}_i \tilde{u}_j$. The trace of the

SGS stress tensor is absorbed into the filtered modified pressure $\tilde{p}^* = \tilde{p}/\rho_0 - p_\infty/\rho_0 + \mathrm{Tr}(\boldsymbol{\tau})/3$, where $\tilde{p}$ is the kinematic pressure and ρ_0 is the air density here 1.225 kg/m^3. The SGS deviatoric stress is modeled using the anisotropic minimum dissipation model (Rozema et al., 2018; Gadde et al., 2021). We use uniform inflow and free-slip boundary conditions with zero vertical velocity at the bottom and top of the domain. The time integration is performed using a third-order accurate Adams-Bashforth scheme. Spatial derivatives in the vertical direction are calculated using a second-order central finite difference scheme. The pseudo-spectral method is applied in the horizontal directions, resulting in periodic boundary conditions in the streamwise and lateral directions.

The computational domain is discretized with n_x, n_y, and n_z points in the streamwise, spanwise, and vertical directions. A uniform grid is used in every direction, with a corresponding grid spacing of $\Delta_x = L_x/n_x$, $\Delta_y = L_y/n_y$, and $\Delta_z = L_z/n_z$, where L_x, L_y, L_z are the dimensions of the computational domain. The computational grid is staggered in the vertical direction. The simulation domain is $L_x \times L_y \times L_z = 8D \times 6D \times 6D$, with D being the rotor diameter. The turbine rotor hub is placed at three diameters after the inlet and in the middle of the y-z plane. This computational setup is based on previous ALM studies (Jha and Schmitz, 2017; Dağ and Sørensen, 2019; Martínez-Tossas et al., 2018; Madsen et al., 2019; Sun et al., 2020; Liu et al., 2022). The employed NREL–5MW (Jonkman et al., 2009) turbine has a rotor diameter of 126 m and we consider a uniform inflow with a velocity of 8 m/s. The rotational speed of the rotor is set to 9.1552 rpm, corresponding to a TSR of 7.55. Three mesh spacings have been used, $\Delta_{\mathrm{grid}} = 4$ m, $\Delta_{\mathrm{grid}} = 2$ m, and $\Delta_{\mathrm{grid}} = 1$ m, which correspond to 31.5, 63, and 126 grid points per turbine diameter. The number of blade points is kept constant at 60. The chord, twist, and aerodynamic coefficient data are interpolated in the radial direction to smooth out discontinuities in the NREL 5MW blade characteristics. We ensure that the statistical stationary state is reached and that the blade tip's movement is less than one grid point for every simulation time step.

6 Validation

6.1 Validation against BEM

The comparison among the classic ALM, the present study ALM, and BEM with tip correction is illustrated in Figure 5. For this analysis, a grid discretization of $\Delta_{\mathrm{grid}} = 2$ m, corresponding to 64 grid points per diameter, is employed. Figure 5a demonstrates that the proposed method converges towards BEM theory with tip corrections. The application of tip correction reduces the axial velocity near the tip, leading to a decreased angle of attack. This finding aligns with experimental evidence, which shows that the downwash caused by pressure equalization diminishes the effective angle of attack at the wingtip (Green, 1995). Moreover, both the normal and tangential loads converge towards those predicted by BEM with tip correction. There are small differences between BEM and ALM within the mid-blade region, originating from the different assumptions in BEM and ALM. Specifically, BEM assumes independence among blade points, whereas in ALM blade points influence each other through the flow solver (Liu et al., 2022). Considering that the ratio of tip-corrected to non-tip-corrected velocities approaches to 1 in the mid-blade region, this does not affect the effectiveness of the proposed method.
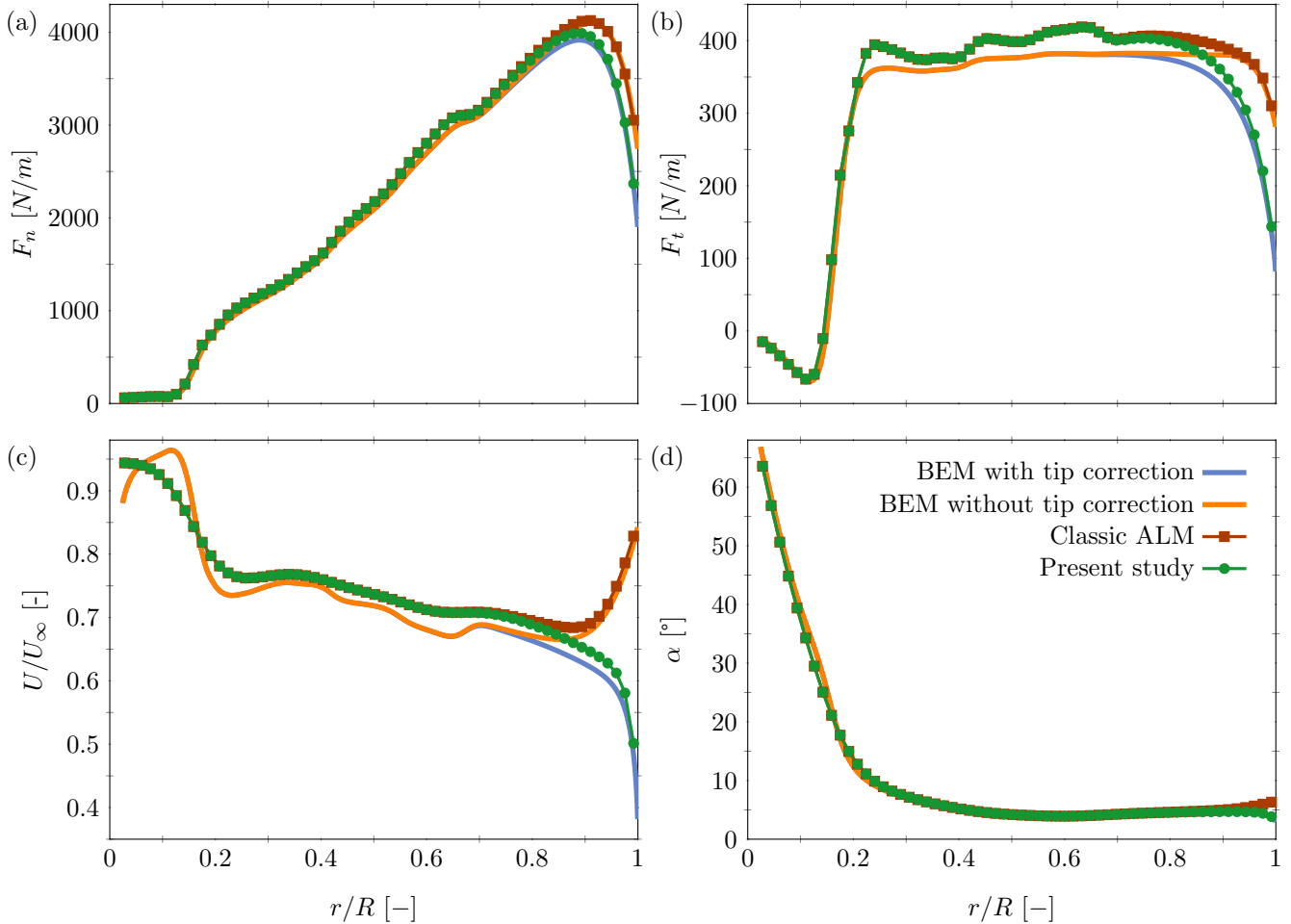
Figure 5. Comparison of the radial distributions of (a) normal and (b) tangential loads, (c) axial velocity component, and (d) angle of attack between classic ALM and the present study ALM (both with $\Delta_{\mathrm{grid}} = 2$ m) and BEM with tip correction.

6.2 Validation against vortex-based smearing correction ALM

175 To further validate our results, we integrated the vortex-based smearing correction method proposed by Meyer Forsting et al. (2019, 2020) into our computational framework; see validation in Appendix A. The integration implemented in our code guarantees that the various ALM versions can be compared accurately, isolating the effect of the methodology. First, we analyse the effect of the vortex-based smearing correction method on the axial velocity. As illustrated in Figure 6c, the axial velocity distribution, in which the correction has been included, closely matches that obtained from BEM with tip correction and present study. Moreover, Figures 6a and 6b demonstrate that the normal and tangential loads calculated by both methods

180 are nearly identical along the entire blade, thus confirming our previous conclusions. We note that the jump in velocity and wind
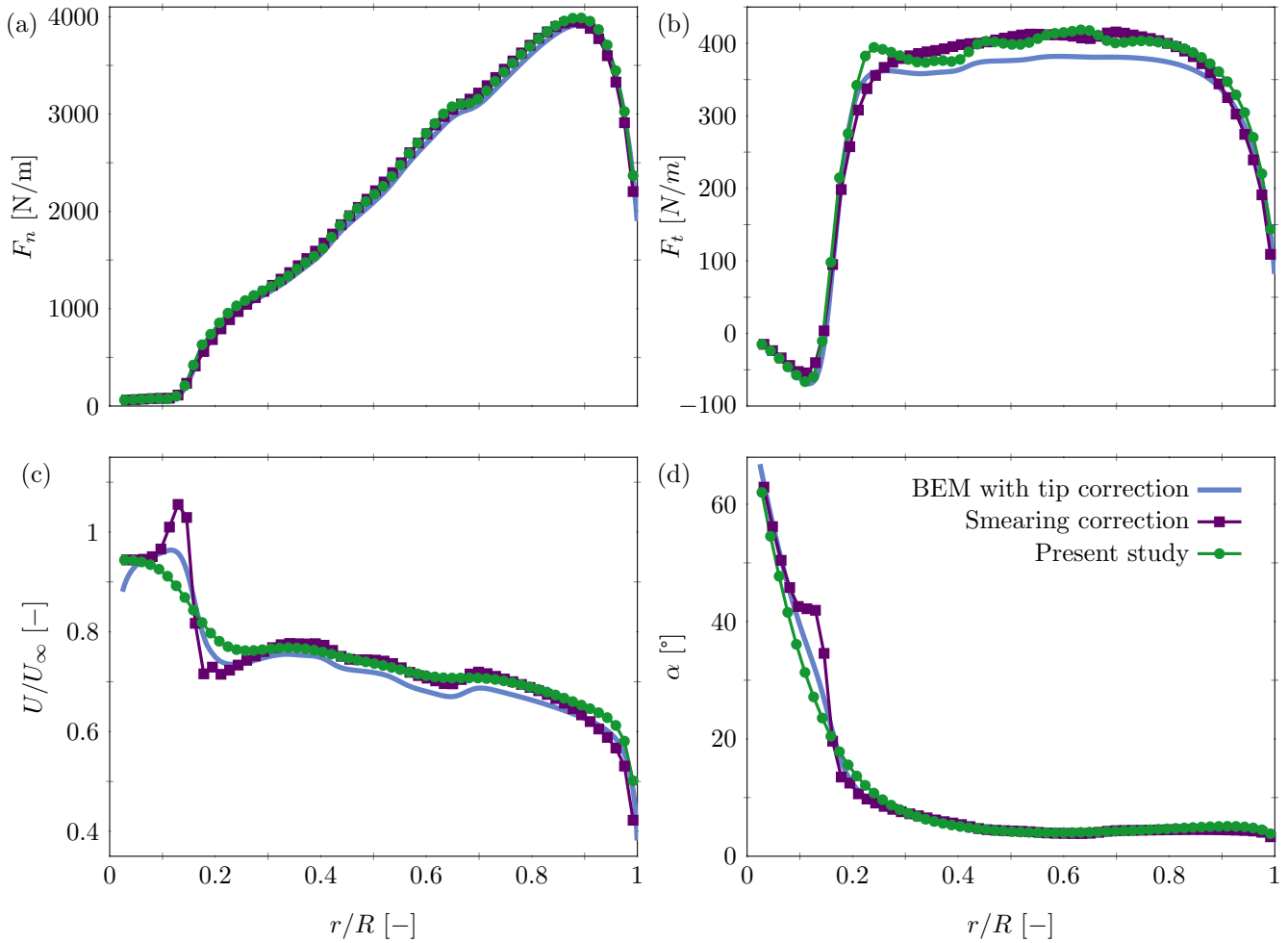
Figure 6. Comparison of the radial distributions of (a-b) normal and tangential loads, (c) axial velocity component, and (d) angle of attack obtained using present study ALM and the vortex-based smearing correction method (both at $\Delta_{\mathrm{grid}} = 2$ m), against BEM with tip correction.

angle near the blade root at $r \approx 0.15R$ in the vortex-based smearing correction method results originate from the employed root correction technique (Pirrung et al., 2016).

6.3 Grid spacing

185 The accuracy of the velocity sampling can be significantly influenced by numerical discretization. As Figure 7 illustrates, the present study ALM converges to BEM with tip correction as the grid spacing (Δ_{grid}) decreases, which is in line with previous findings (Meyer Forsting et al., 2019; Liu et al., 2022). Figure 8 compares the proposed method and the vortex-based smearing correction method for $\Delta_{\mathrm{grid}} = 4$ m. This shows that the vortex-based smearing correction yields more consistent results across various grid resolutions as the results are similar to the $\Delta_{\mathrm{grid}} = 2$ m results shown in Figure 6. This consistency with grid
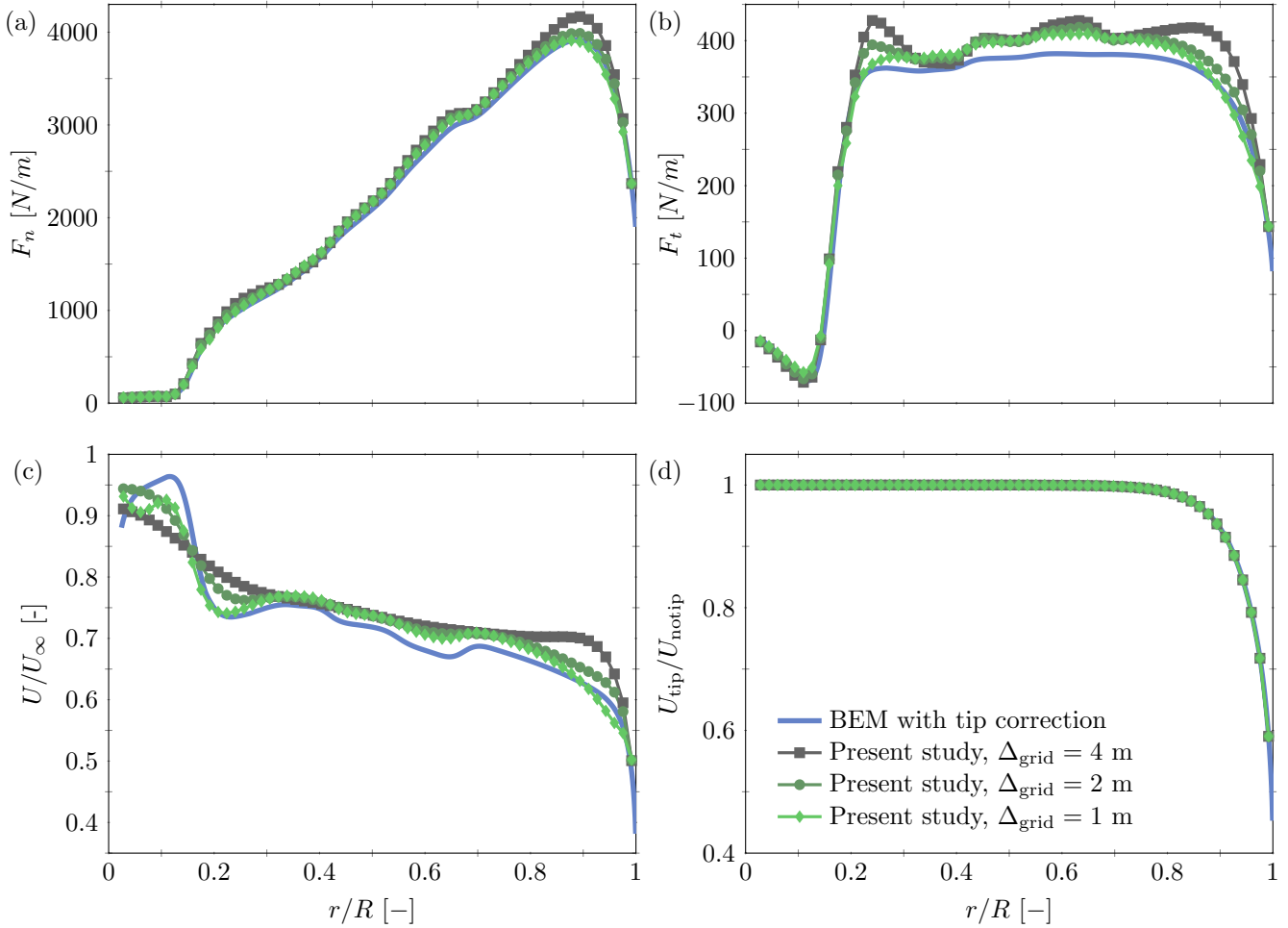
Figure 7. Comparison of the radial distribution of the (a) normal loads, (b) tangential loads, (c) axial velocity, and (d) the computed velocity ratios (see Equation 13) obtained using the presented study ALM at grid discretizations of $\Delta_\mathrm{grid} = 4$, 2, and 1 m with BEM theory incorporating tip correction.

resolution can be attributed to the employed empirical models, a point highlighted by Pirrung et al. (2017). The results from the present study ALM appear more susceptible to changes in grid resolution.

The relative difference between the power (C_P) and thrust (C_T) coefficients, obtained from the proposed correction and using the vortex-based smearing correction method compared to the BEM theory with tip correction, is presented in Table 1. At the finest grid spacing, the difference between the present study ALM and BEM reduces to 4.3% for the power coefficient (C_P) and 0.7% for the thrust coefficient (C_T). It is important to recognize that perfect convergence is not anticipated due to the previously discussed inherent differences between the BEM and ALM (see also Liu et al. (2022)). The present study ALM significantly outperforms classic ALM method by almost halving the percentage errors. The vortex-based smearing correction

Table 1. Convergence of the thrust and power coefficients from the present study ALM and the vortex-based smearing correction method with mesh refinement towards those predicted by BEM theory.

Simulation	C_P	Error %	C_T	Error %
BEM with tip correction	**0.4898**		**0.7892**	
Present study, $\Delta_{\mathrm{grid}} = 4$ m	0.54	11.0	0.82	3.6
$\Delta_{\mathrm{grid}} = 2$ m	0.52	6.9	0.80	2.0
$\Delta_{\mathrm{grid}} = 1$ m	0.51	4.3	0.79	0.7
Smearing correction, $\Delta_{\mathrm{grid}} = 4$ m	0.51	5.4	0.80	1.6
$\Delta_{\mathrm{grid}} = 2$ m	0.52	5.1	0.80	1.3
Classic ALM, $\Delta_{\mathrm{grid}} = 2$ m	0.55	13.2	0.82	4.0
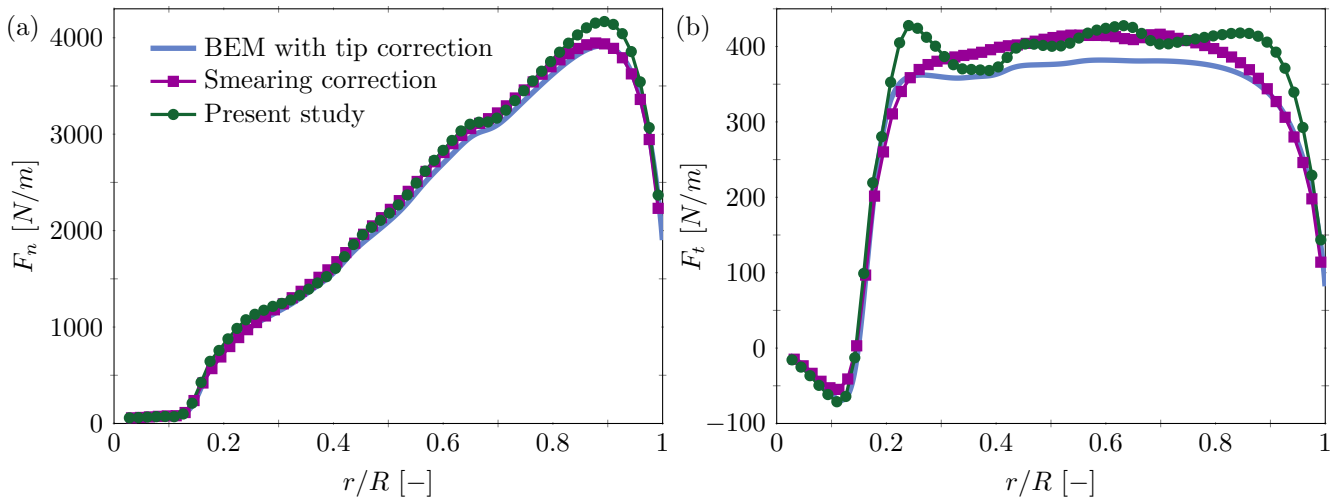
Figure 8. Comparison of the radial distributions of (a) normal and (b) tangential loads among the present study ALM, the vortex-based smearing correction method (both utilizing $\Delta_{\mathrm{grid}} = 4$ m), and BEM with tip correction.

method Meyer Forsting et al. (2019) shows even better performance, particularly on coarser meshes. However, crucial strengths of the present study correction include its straightforward implementation, lower computational overhead, and the coupling with the widely used BEM framework. Since the proposed correction is based on the BEM framework, it allows for the direct integration of existing tip corrections (Crawford, 2006; Madsen et al., 2010; Sørensen, 2016), thereby enhancing the versatility of the proposed method.

Table 2. Parameters adopted for the simulations with varying inflow velocities.

$\mathbf{U}_\infty$ [m/s]	Ω [rpm]	TSR	θ [°]
4.0	7.190	11.86	0
5.5	7.707	9.25	0
7.0	8.465	7.98	0
8.5	9.727	7.55	0
10.0	11.444	7.55	0
11.5	12.073	6.92	1.283
13.0	12.073	6.13	6.560
14.5	12.073	5.49	9.529
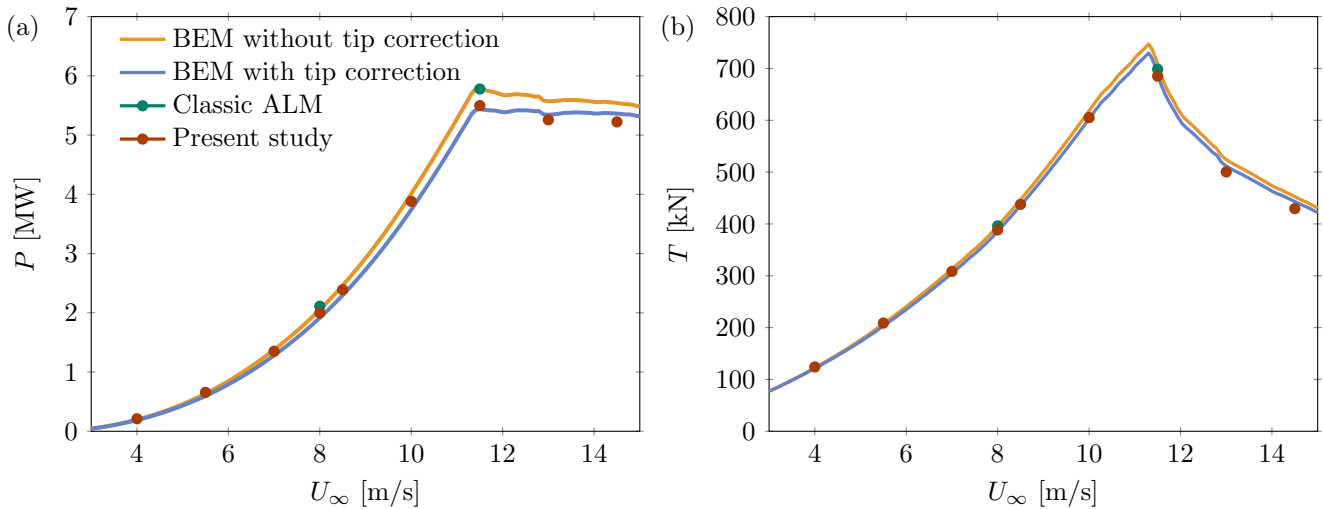
Figure 9. Comparison of rotor generated power (a) and thrust (b) for different inflow velocities among the present study ALM (utilizing $\Delta_{\mathrm{grid}} = 1$ m) and BEM with tip correction.

6.4 Inflow velocity

To study the performance of the proposed method under varying inflow conditions, we simulate the NREL 5MW turbine at
205 different inflow velocities. Adopting $\Delta_{\mathrm{grid}} = 1$ m, we perform eight additional simulations with inflow velocity ranging from 4
to 14.5 m/s. The corresponding TSR, angular velocity and pitch angle θ are reported in table 2 and obtained from Jonkman et al.
(2009). Figure 9 shows the comparison among the present ALM, BEM with tip correction, classic ALM and BEM without tip

correction. The agreement between the proposed method and BEM with tip correction is excellent for all inflow velocities. This demonstrates the robustness of the proposed algorithm across a wide range of flow conditions, underlying the possibility of

210 employing the proposed correction in various flow scenarios. Furthermore, even with the relatively fine grid spacing adopted, the present study ALM still outperforms the classic ALM and BEM without tip correction at all velocities, especially regarding the rotor power, in which the maximum difference between the classic ALM and the present study ALM is 5% at 11.5 m/s. The rotor thrust is also improved, however at this discretization the classic ALM deviates less with respect to BEM without tip correction.

7 Conclusions

We introduce a velocity correction for the Actuator Line Method (ALM), which is intended to address the limitations commonly associated with the classic ALM approach. The correction's algorithm leverages BEM theory to determine the ratio between tip-corrected and non-tip-corrected velocity components at the rotor blades, which is then used to correct the velocities sampled at the blades. This adjustment aligns the angle of attack, wind direction, and loads derived from ALM with those predicted by

220 BEM theory incorporating tip correction. Since this method requires only the TSR as input, it can be easily applied to various flow scenarios, including simulations of wind farms, as it is possible to estimate the TSR associated to each turbine. The benefits of the present study ALM are its straightforward implementation, minimal computational overhead, and consistency with the widely used BEM framework, which ensures broad applicability. The approach has been validated against the vortex-based smearing correction method by Meyer Forsting et al. (2019, 2020), which uses a different technique for velocity correction,

225 thereby demonstrating the consistency and reliability of our method.

Appendix A: Appendix A

Figure A1 compares the results from our simulations with the distribution digitally extracted from Meyer Forsting et al. (2019), under identical conditions: $U_\infty = 8$ m/s, $\Omega = 9.2$ rpm, 19 actuator points, and $\Delta_{\text{grid}} = R/40 \approx 1.6$ m. The smearing length is defined as $\varepsilon = 2\Delta_{\text{grid}}$. This comparison illustrates that the two codes agree, and the results from Meyer Forsting et al.

230 (2019) align with the BEM theory with tip correction, thereby validating the latter as a reliable reference. We attribute the observed differences for tangential force in the mid-blade region to differences in the flow solvers (RANS and LES), or specific implementation details of the ALM. These discrepancies do not affect the comparisons presented in the main text, which are all conducted within the same simulation framework.

Author contributions. D. Selvatici: conceptualization, data curation, formal analysis, investigation, methodology, software, validation, writ-

235 ing - original draft and review & editing. R.J.A.M. Stevens: conceptualization, funding acquisition, investigation, project administration, software, supervision, writing - review & editing.
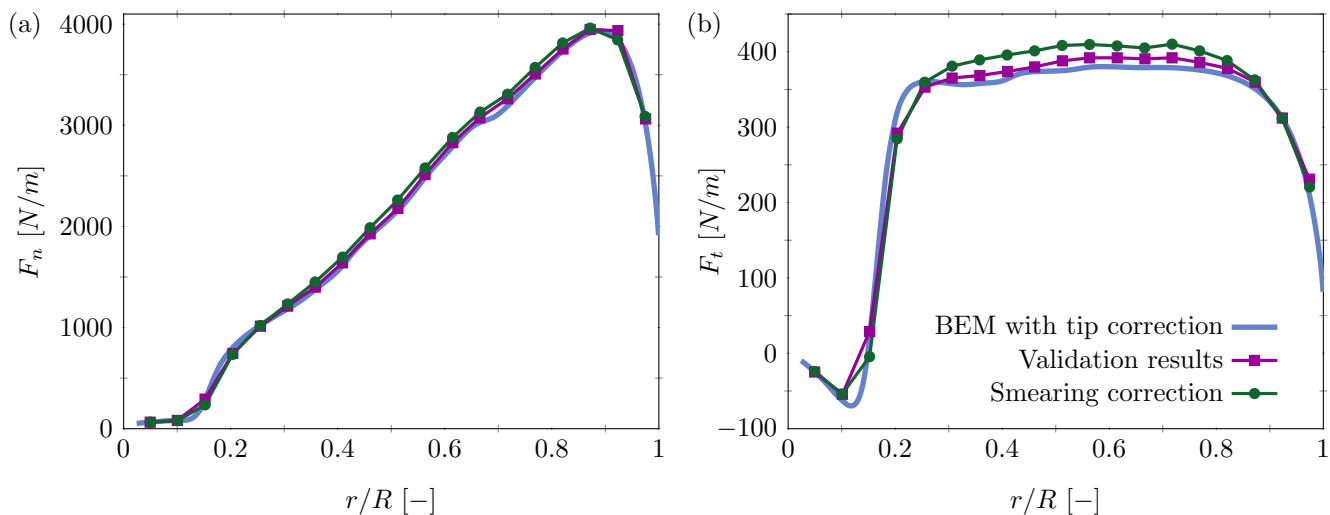
Figure A1. Comparison of the radial distributions of (a) normal and (b) tangential loads as obtained by vortex-based smearing correction method by Meyer Forsting et al. (2019) (digitally extracted), their methodology integrated in our code, and BEM with tip corrections.

Competing interests. The authors declare that they have no conflict of interest.

Acknowledgements. This project has received funding from the European Research Council under the European Union's Horizon 2020 research and innovation program (Grant No. 804283). This work was partly carried out on the Dutch national e-infrastructure with the support of SURF Cooperative. We acknowledge the EuroHPC Joint Undertaking for awarding the project EHPC-REG-2023R03-178 access to the EuroHPC supercomputer Discoverer, hosted by Sofia Tech Park (Bulgaria).

240

References

Albertson, J. D.: Large Eddy Simulation of Land-Atmosphere Interaction, Ph.D. thesis, 1996.

Bangga, G.: Comparison of Blade Element Method and CFD Simulations of a 10 MW Wind Turbine, Fluids, 3, 2018.

245 Bangga, G. and Lutz, T.: Aerodynamic modeling of wind turbine loads exposed to turbulent inflow and validation with experimental data, Energy, 223, 2021.

Branlard, E.: Wind Turbine Aerodynamics and Vorticity-Based Methods, Springer, 2017.

Buhl, M. L.: A New Empirical Relationship between Thrust Coefficient and Induction Factor for the Turbulent Windmill State, Tech. rep., National Renewable Energy Laboratory, 2005.

250 Churchfield, M. J., Schreck, S., Martínez-Tossas, L. A., Meneveau, C., and Spalart, P. R.: An Advanced Actuator Line Method for Wind Energy Applications and Beyond, https://doi.org/10.2514/6.2017-1998, aIAA SciTech Forum, 2017.

Crawford, C.: Re-examining the precepts of the blade element momentum theory for coning rotors, Wind Energy, 9, 457–478, 2006.

Dağ, K. O. and Sørensen, J. N.: A new tip correction for actuator line computations, Wind Energy, 23, 148–160, 2019.

Diaz, G. P. N., Otero, A. D., Asmuth, H., Sørensen, J. N., and Ivanell, S.: Actuator line model using simplified force calculation methods,
255 Wind Energy Sci., 8, 363–382, 2023.

Gadde, S. N., Stieren, A., and Stevens, R. J. A. M.: Large-Eddy Simulations of Stratified Atmospheric Boundary Layers: Comparison of Different Subgrid Models, Bound.-Layer Meteorol., 178, 363–382, 2021.

Glauert, H.: Airplane Propellers, Springer, 1935.

Green, S. I.: Wing Tip Vortices. Fluid Mechanics and Its Applications, Springer, 1995.

260 Jha, P. K. and Schmitz, S.: Actuator curve embedding – an advanced actuator line model, J. Fluid Mech., 834, 2017.

Jha, P. K., Churchfield, M. J., Moriarty, P. J., and Schmitz, S.: Guidelines for Volume Force Distributions Within Actuator Line Modeling of Wind Turbines on Large-Eddy Simulation-Type Grids, J. Sol. Energy Eng., 136, 2014.

Jonkman, J., Butterfield, S., Musial, W., and Scott, G.: Definition of a 5-MW Reference Wind Turbine for Offshore System Development, Tech. rep., National Renewable Energy Laboratory (NREL), 2009.

265 Liu, L., Franceschini, L., Oliveira, D. F., Galeazzo, F. C. C., Carmo, B. S., and Stevens, R. J. A. M.: Evaluating the accuracy of the actuator line model against blade element momentum theory in uniform inflow, Wind Energy, 25, 1046–1059, 2022.

Madsen, H. A., Bak, C., Døssing, M., Mikkelsen, R., and Øye, S.: Validation and modification of the Blade Element Momentum theory based on comparisons with actuator disc simulations, Wind Energy, 13, 373–389, 2010.

Madsen, M. H. A., Zahle, F., Sørensen, N. N., and Martins, J. R. R. A.: Multipoint high-fidelity CFD-based aerodynamic shape optimization
270 of a 10 MW wind turbine, Wind Energy Sci., 4, 163–192, 2019.

Martínez-Tossas, L. A., Churchfield, M. J., Yilmaz, A. E., Sarlak, H., Johnson, P. L., Sørensen, J. N., Meyers, J., and Meneveau, C.: Comparison of four large-eddy simulation research codes and effects of model coefficient and inflow turbulence in actuator-line-based wind turbine modeling, Renew. Sustain. Energy Rev., 10, 2018.

Martínez-Tossas, L. A., Churchfield, M. J., and Meneveau, C.: Optimal smoothing length scale for actuator line models of wind turbine
275 blades based on Gaussian body force distribution, Wind Energy, 20, 1083–1096, 2017.

Melani, P. F., Mohamed, O. S., Cioni, S., Balduzzi, F., and Bianchini, A.: An insight into the capability of the actuator line method to resolve tip vortices, Wind Energy Sci., 9, 601–622, 2024.

Meyer Forsting, A. R., Pirrung, G. R., and Ramos-García, N.: A vortex-based tip/smearing correction for the actuator line, Wind Energy Sci., 4, 369–383, 2019.

280 Meyer Forsting, A. R., Pirrung, G. R., and Ramos-García, N.: Brief communication: A fast vortex-based smearing correction for the actuator line, Wind Energy Sci., 5, 349–353, 2020.

Ning, S. A.: A simple solution method for the blade element momentum equations with guaranteed convergence, Wind Energy, 17, 1327–1345, 2013.

Pirrung, G. R., Madsen, H. A., Kim, T., and Heinz, J.: A coupled near and far wake model for wind turbine aerodynamics, Wind Energy, 19, 2053–2069, 2016.

285

Pirrung, G. R., Madsen, H. A., and Schreck, S.: Trailed vorticity modeling for aeroelastic wind turbine simulations in standstill, Wind Energy Sci., 2, 521–532, 2017.

Rozema, W., Verstappen, R. W. C. P., Veldman, A. E. P., and Kok, J. C.: Low-Dissipation Simulation Methods and Models for Turbulent Subsonic Flow, Arch. Comput. Methods Eng., 27, 299–330, 2018.

290 Shen, W. Z., Sørensen, J. N., and Mikkelsen, R.: Tip Loss Correction for Actuator/Navier–Stokes Computations, J. Sol. Energy Eng., 127, 209–213, 2005.

Stevens, R. A. M., Wilczek, M., and Meneveau, C.: Large-eddy simulation study of the logarithmic law for second- and higher-order moments in turbulent wall-bounded flow, J. Fluid Mech., 757, 888–907, 2014a.

Stevens, R. J. A. M., Graham, J., and Meneveau, C.: A concurrent precursor inflow method for Large Eddy Simulations and applications to

295 finite length wind farms, Renew. Energy, 68, 46–50, 2014b.

Sun, Z., Zhu, W. J., Shen, W. Z., Zhong, W., Cao, J., and Tao, Q.: Aerodynamic Analysis of Coning Effects on the DTU 10 MW Wind Turbine Rotor, Energies, 13, 2020.

Sørensen, J. N.: General Momentum Theory for Horizontal Axis Wind Turbines, Springer, 2016.

Sørensen, J. N. and Shen, W. Z.: Numerical Modeling of Wind Turbine Wakes, J. Fluids Eng., 124, 393–399, 2002.

300 Troldborg, N.: Actuator Line Modeling of Wind Turbine Wakes, Ph.D. thesis, Technical University of Denmark, 2008.